Multiple Chord Measurements of Two Centaurs by Stellar Occultation

Ryder H. Strauss[1]

[1]*Department of Astrophysical and Planetary Sciences*
University of Colorado Boulder
2000 Colorado Ave,
Boulder, CO 80309, USA

ABSTRACT

Stellar occultation is a high-precision technique for obtaining measurements of the geometry of small bodies of the solar system. The Research and Education Collaborative Occultation Network (RECON) is a network designed to observe high-uncertainty occultations by the most distant of these objects: trans-neputnian objects (TNOs). In the year 2019, among other occultation results, RECON obtained multiple-chord occultation measurements of two TNOs, both part of the Centaur population. These measurements provide geometric and astrometric constraints to these objects at a very high precision. This paper reports the methods and results of these two occultation efforts.

Thesis Advisor

Dr. John Keller - Dept. of Astrophysical and Planetary Sciences

Thesis Committee

Dr. Ann-Marie Madigan- Dept. of Astrophysical and Planetary Sciences, JILA

Dr. Bethany Wilcox - Dept. of Physics

Dr. Seth Hornstein - Dept. of Astrophysical and Planetary Sciences

Dr. John Keller - Dept. of Astrophysical and Planetary Sciences

Defense date: 30 March 2020

1. INTRODUCTION

The small bodies of the outer solar system are an incredibly important population to study in the realm of solar system science. Kuiper Belt Objects (KBOs) are thought to be among the most primordial objects in the solar system. The sparse environment in the outermost solar system means that interactions are very infrequent. The most compelling evidence for the primordial nature of these objects is the observations of the surface of the classical KBO Arrokoth during the flyby by the New Horizons spacecraft. Arrokoth appears to consist of a number of subsections which look to have gently accreted together . Additionally, the surface of the object is smooth and lightly cratered, but the density of craters is consistent with a ¿4 billion year-old surface (Spencer et al. 2020). For these reasons, it is likely that this object has existed much as it is since the early accretionary solar system. In learning about the physical properties of these bodies, we stand to gain valuable insight into the composition and origin of planetesimals in the infant solar system.

Of equal interest to those studying the origins of the solar system via the KBO population is the population of Centaurs - objects with orbits in between the giant planets in the outer solar system. Dynamical simulations show that these orbits are unstable, with very short dynamical lifetimes - the ensemble half-life of the entire population is only 2.7 million years (Horner et al. 2004). Additionally, the population of Centaurs have a similar size, albedo, and color distribution to KBOs (Tegler et al. 2016). This suggests that the majority of the Centaur population likely have their origins in the Kuiper belt.

Due to their small size, low brightness, and distance from the Earth, these trans-neptunian objects (TNOs) are difficult to probe via direct measurement. While some low-precision information about size and albedo can be determined via infrared thermal imaging (Lebofsky & Spencer 1989), stellar occultations are a considerably higher- precision method of obtaining these measurements. The highest precision technique is, of course, a spacecraft flyby, but these are incredibly expensive compared to the small ground-based telescope campaigns required to observe an occultation. When an object occults a distant star, the drop in the flux from that star can be recorded to generate a lightcurve, and the duration of that drop provides a very accurate measurement of the width along a specific chord of the object. If multiple stations spaced across the path of the object's shadow observe the occultation, multiple chords across the object are measured, and a model of the two-dimensional profile of the object can begin to be fitted to the lightcurve data.

Due to the large uncertainties in the orbit fits for these objects, occultations by outer solar system objects are difficult to measure - much more so than occultations by main-belt asteroids, such as the three high-precision asteroid occultations discussed in Timerson et al. (2009). Optical telescope astrometry can only be acquired to a certain angular precision; at the distance of these objects, a given angular uncertainty (roughly 5 milli-arcseconds for astrometry from Chambers et al. (2016)) corresponds

to a much larger uncertainty in the plane of the sky than the same angular uncertainty at the distance of the main belt. The Research and Education Collaborative Occultation Network (RECON) is a network of telescopes designed with this problem in mind. RECON is a stationary network of volunteer citizen astronomer sites set up as a 61-station "picket fence" along the entire western edge of the United States, extending 2000 km in the north-south direction, with the intent of observing these large-uncertainty occultations with a reasonable probability of success (Buie & Keller 2016). In recent years, RECON has been supplemented by a Canadian extension to the network, named "CanCON."

As of the end of 2018, occultation measurements of only six objects from the Centaur population had been obtained (Braga-Ribas et al. 2019). In 2019, RECON made multiple chord occultation measurements of two additional Centaurs, bringing this number to eight. These detections are the subject of this paper. On 28 January 2019, two chords were measured across a Centaur with the designation 2014 YY49. On 4 September 2019, three chords were measured across a second Centaur designated 2013 NL24.

This paper presents the results from both of these occultation measurements. It is organized such that the two occultations are presented in parallel, from prediction to results. Section 2 describes the predictions for the occultation events. Section 3 details the observation efforts for the two events. Section 4 describes the method and results of the photometric analysis of the data from these events. Section 5 details the method used for the profile fitting of each object, and the results of these modeling efforts. Section 6 provides a discussion of the results, implications, and future research.

2. PREDICTIONS

2.1. *2014 YY49*

An occultation between the Centaur 2014 YY49 and the Gaia DR2 star GA 3318035546681086336 (Lindegren et al. 2018) at 05:08:56 on 2019/01/28 UT was identified by the RECON prediction system, which automatically calculates appulses and selects those which may result in occultations observable by the RECON network. This target was discovered by Pan-STARRS (Chambers et al. 2016) in 2014, with observations recovered back through 2004. Recent measurements taken by the RECON project with the ARC 3.5m telescope at Apache Point Observatory reduced the astrometric uncertainty sufficiently such that an observable occultation prediction could be generated. The 1-sigma time uncertainty for this prediction was 48 seconds, and the 1-sigma cross-track uncertainty was 738 km, with the nominal shadow path passing directly over central Washington. The RECON network spanned $+0.3\sigma$ to the north, and -1.5σ to the south in the cross-track direction. Figure 1 shows the geometry of the occultation prediction on the Earth. With an absolute magnitude of $H_v = 10.8$, the diameter of the object was predicted to have a lower limit of 22.5km assuming a 30% geometric albedo. With a median site spacing of 18.2km in the cross-track direction, the probability of at least one detection (assuming 100% network participation by all 61 teams) was 45.5%. Details of the occulted star are summarized in table 1. A summary of prediction details can be found in Table 3.

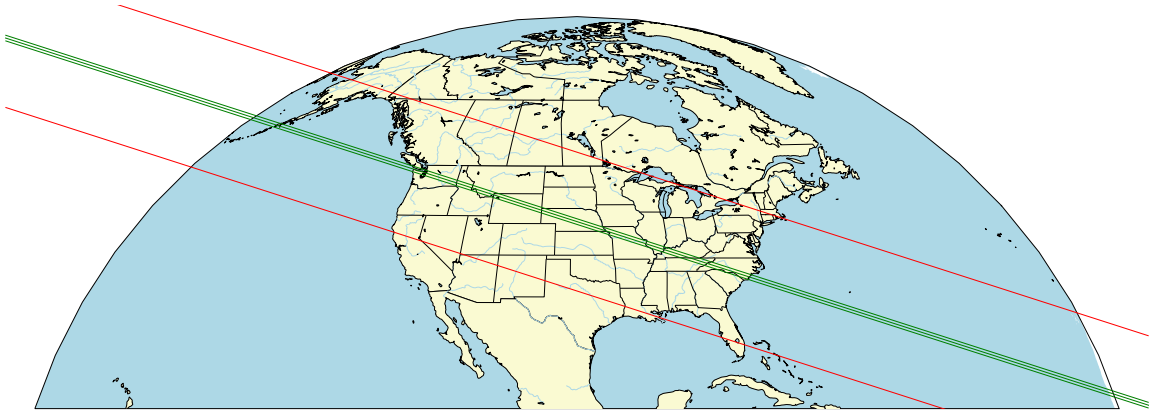

Figure 1. The predicted shadow track for the occultation by 2014 YY49 on 28 January 2019 UT. The green lines show the nominal centerline and cross-track extent of the object. The red dashed lines indicate the 1-sigma uncertainties in the cross-track direction of the prediction.

Table 1. Parameters for the star occulted by 2014 YY49

Star Details from Gaia DR2	
Star Gaia DR2 source id	3318035546681086336
Reference epoch (Julian Year in TCB)	2015.5
α	104.98120062043789 ° ± 0.035 mas
δ	1.4238945541698338 ° ± 0.032 mas
Proper motion α (mas yr^{-1})	-0.81 ± 0.06
Proper motion δ (mas yr^{-1})	0.49 ± 0.06
Parallax p (mas)	0.38 ± 0.04
G_{mag}	14.5
Systematic Uncertainties from Gaia DR2	
Proper motion σ_{pm} (mas yr^{-1})	0.066
Parallax σ_{plx} (mas)	0.043
Star Astrometric Position at Time of Occultation	
α_{ast}	1.4238950070 ° ± 0.326 mas
δ_{ast}	104.9811997733 ° ± 0.329 mas

NOTE—Star astrometric parameters are from Gaia DR2 catalog with position in ICRS at the catalog reference epoch. The star astrometric position includes proper motion and parallax correction for the time of the occultation t_0=2019-01-28 05:08:56 UTC. The propagated uncertainties in RA and DEC include the uncertainties from position, proper motion and parallax plus GDR2 systematic uncertainties in proper motion and parallax from Lindegren et al. (2018).

2.2. *2013 NL24*

The automated RECON prediction system identified an appulse between the Gaia catalog star GA 2601908921837308672 (Lindegren et al. 2018) and the Centaur 2013 NL24, and a prediction was generated for an occultation which would take place at 07:10:47 on 2019/09/04 UTC. This object was discovered by the Pan-STARRS project in 2013, with measurements recovered back through 2010. All astrometry informing this prediction was obtained by the Pan-STARRS project (Chambers et al. 2016). The 1-sigma time uncertainty for this prediction was 74 seconds, and the 1-sigma cross-track uncertainty was 1195 km, with the nominal centerline passing over the Canadian sites at the northernmost end of the joint RECON/CanCON network (geometry shown in figure 2). The network spanned +0.023σ to the north, and -0.98σ to the south in the cross-track direction. In the down-track direction, we asked that each team record for ±5σ. With an absolute magnitude of $H_v = 8.2$, the diameter of the Centaur was predicted to have a lower limit of 55.6km assuming a 30% geometric albedo. With a median site spacing of 12.6km in the cross-track direction, the probability of detection was 26.3%. Details of this prediction are summarized in table 3. Details of the occulted star are summarized in table 2.

Table 2. Parameters for the star occulted by 2013 NL24

Star details from Gaia DR2	
Star Gaia DR2 source id	2601908921837308672
Reference epoch (Julian Year in TCB)	2015.5
α	338.3818086358572 ° ± 0.053 mas
δ	-11.3721979521263 ° ± 0.045 mas
Proper motion α (mas yr^{-1})	0.9 ± 0.1
Proper motion δ (mas yr^{-1})	-4.19 ± 0.08
Parallax p (mas)	0.41 ± 0.06
G_{mag}	15.6
Systematic Uncertainties in Gaia DR2	
Proper motion σ_{pm} (mas yr^{-1})	0.066
Parallax σ_{plx} (mas)	0.043
Star Astrometric Position at Time of Occultation	
α_{ast}	338.3818075337 ° ± 0.449 mas
δ_{ast}	-11.3722028193 ° ± 0.554 mas

NOTE—Star astrometric parameters are from Gaia DR2 catalog with position in ICRS at the catalog reference epoch. The star astrometric position includes proper motion and parallax correction for the time of the occultation t_0=2019-09-04 07:10:47 UTC. The propagated uncertainties in RA and DEC include the uncertainties from position, proper motion and parallax plus GDR2 systematic uncertainties in proper motion and parallax from Lindegren et al. (2018).

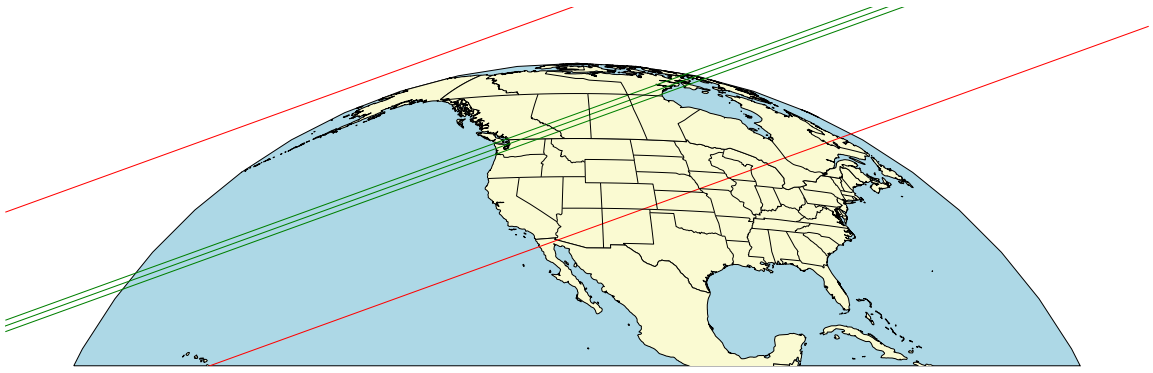

Figure 2. The predicted shadow track for the occultation by 2013 NL24 on 4 September 2019 UT. The green lines show the nominal centerline and cross-track extent of the object. The red dashed lines indicate the 1-sigma uncertainties in the cross-track direction of the prediction.

Table 3. Prediction Details for both Centaur occultations

	2014 YY49	2013 NL24
Geocentric closest approach t_0	2019/01/28 05:08:56 UTC	2019/09/04 07:10:47 UTC
Sky plane scale (km/")	12919.9	18627.1
v_{occ} (km/sec)	21.5	22.9
Cross track uncertainty (km)	738	1195
Time uncertainty (s)	48	74
H_v	10.2	8.2
V-mag	23.0	22.4
Distance to Object (AU)	17.8	25.7
Moon elongation (°)	116	107
Moon illumination(%)	47	31

NOTE—the H_v adopted here is that provided by the Minor Planet Center. There are no formal uncertainties reported on this value, and it is generated from a varied set of measurements, so it will not be used in the formal analysis in this paper.

3. OBSERVATIONS

3.1. *2014 YY49*

This event was observed as an official campaign for RECON. Thirty-six teams attempted to observe this occultation. 33 of these teams attempted to record using the standard RECON recording setup detailed in Buie & Keller (2016). The remaining teams (namely the CanCON teams) used a different configuration involving a new QHY-174m CMOS camera. Each team was asked to record the target field for a duration of 5 sigma about the nominal time in the down-track direction. Nominally, each RECON team was to record at a Sense-Up of x64 ($\sim$ 1 second exposures), which would ensure a sufficient compromise between signal to noise and temporal resolution. A number of teams recorded using Sense-Ups as high as x128 ($\sim$ 2 second exposures), based on the sky conditions at their respective locations. Of the 36 teams who attempted to observe this occultation, 23 successfully recorded the target star at the predicted time of the occultation to provide constraining data on the target. Of the remaining 13 teams, 3 recorded the incorrect field, 6 were unable to collect good data due to sky conditions, and 4 were unable to record due to technical issues. A summary of observers is provided in table 4. A map showing RECON's coverage of this event is shown in figure 3.

Table 4. Participating Sites

SiteID	UT start	UT end	SUP	Lat	Lon	Alt	Q	Observers	Comment
1-03 Burney	05:06:46	05:15:50	64	+40.873853	-121.652450	965	2	M. von Schalscha	Field not visible until end
1-04 Susanville	05:06:36	05:15:10	128	+40.367067	-120.672992	1293	1	B. Bateson	Clouds for most of video
1-06 Quincy	05:06:43	05:15:43	128	+39.944464	-120.946723	1039	4	R. Logan, W. Anderson	Longer exposure due to clouds
1-07 Portola	05:06:40	05:15:47	128	+39.794077	-120.656105	1365	1	C. Callahan, M. Callahan, S. Callahan	Intermittent clouds throughout
1-08 Reno	05:06:15	05:15:44	64	+39.391243	-119.764687	1456	5	T. Stoffel, L. Loftin, B. Crosby	
1-09 Carson City	05:06:37	05:15:49	64	+39.185632	-119.796428	1516	5	I. Pettersen, L. Hemingway, J. Bean, L. Rodriguez, L. Woods, J. Blackeye, M. Ramirez, M. Fontaine	
1-10 Yerington	···	···	···	(+38.991111)	(-119.160833)	(1340)	0	T. Hunt	Telescope error
1-13 Bishop	05:06:30	05:15:32	128	+37.483987	-118.606792	1552	4	J. Slovacek	
1-14 CPSLO	05:06:38	05:15:40	128	+35.300500	-120.659833	109	4	M. Kehrli, D. Swanson, S. Hopfe	Position from Logsheet
2-04 Indian Springs	05:06:32	05:15:23	64	+36.440363	-115.357632	885	5	S. Bock, J. Heller, T. Garcia, N.Service	
2-07 Kingman	05:04:03	05:16:03	64	+35.189333	-114.053000	1016	0	K. Pool, F. Gilbert, R. Cox, C. Lucier	Wrong Field Recorded
2-09 Mohave Valley	05:06:06	05:15:20	64	+35.031753	-114.596695	153	5	J. White	
2-10 Lake Havasu City	···	···	···	(+34.494235)	(-114.317889)	(259)	0	S. Chase	Bad weather
2-11 Parker	05:06:06	05:15:33	128	+34.141092	-114.288323	103	5	R. Reaves	
2-13 Blythe	05:06:17	05:15:16	64	+33.607970	-114.577887	51	5	D. Barrows, N. R. Patel, L.-E. Pope	LC shows field adjustments

Table 4 *continued on next page*

Table 4 *(continued)*

SiteID	UT start	UT end	SUP	Lat	Lon	Alt	Q	Observers	Comment
2-15 Yuma	05:05:58	05:15:18	64	+32.663785	-114.559340	30	5	D. Thompson, D. Conway, M. Echols, K. Conway, K. Mclelland, R. Quinn, M. Echols	
2-16 Tonasket	···	···	···	(+48.701342)	(-119.434454)	(316)	0	E. Bjelland	Technical Issues
2-19 Ellensburg	05:06:41	05:15:48	64	+47.002215	-120.540178	489	4	D. Marshall, C. Fallscheer, H. Seemiller, K. McKeowm, M. Rivard, P. Zencak	Poor focus in video
2-21 The Dalles	···	···	···	(+45.596173)	(-121.188597)	(77)	0	B. Dean, M. Dean	Bad weather
2-23 Sisters	05:05:22	05:16:10	128	+44.296307	-121.577312	984	4	R. Givot, J. Hammond, R. Thorklidson, R. Schar, D. McCrystal, A. Hills, L. Miller, P. Mendoza	LC shows field adjustments
2-24 Bend	05:06:25	05:16:30	64	+44.132712	-121.331572	976	5	A.-M. Eklund, L. Matheny	
2-26 North Lake	···	···	···	(+43.245017)	(-120.902688)	(1345)	0	S. Spurgeon	Faulty video cable
2-27 Paisley	···	···	···	(+42.693379)	(-120.542721)	(1329)	0	J. Garland	Technical Issues
2-29 Klamath Falls	05:03:52	05:16:20	64	+42.242455	-121.780930	1280	5	S. Anthony, Y. Yang, I. Klopf, H. Yang	
3-02 Okanogan	05:01:38	05:17:09	64	+48.362438	-119.596937	293	5	D. Colbert, J. Cheeseman	
3-05 Yakima	05:08:09	05:18:34	64	+46.588887	-120.567945	332	5	M. Meyer, B. Palmquist	Wrong field until 05:11
3-06 Goldendale	05:08:43	05:15:42	64	+45.853602	-120.760572	616	5	S. Wanderscheid	Partial recording
3-07 Maupin	05:06:43	05:15:44	64	+45.177547	-121.079652	293	5	J. Sowell, J. Popchock	
C-01 Oliver	···	···	···	(+49.181172)	(-119.558915)	(331)	0	S. McIntyre	Wrong field
C-05 Summerland	···	···	···	(+49.599999)	(-119.670005)	(485)	0	Dave Gamble	Unable to Acquire field
C-06 Anarchist	···	···	1s*	+49.008842	-119.363005	1052	5	D. Ceravolo, P. Ceravolo	Recorded with QHY174M
L-03 SwRI	···	···	···	(+40.003545)	(-105.263038)	(1624)	0	NULL	bad weather

Table 4 *continued on next page*

Table 4 *(continued)*

SiteID	UT start	UT end	SUP	Lat	Lon	Alt	Q	Observers	Comment
V-01 Gardnerville	05:06:37	···	32	+38.889892	-119.672293	1520	5	J. Bardecker	Issues with dropped frames
V-04 Oregon Obs	05:05:11	05:16:36	64	+43.885343	-121.447895	1242	5	B. Thomas	
V-05 Scottsdale	05:05:41	05:15:40	16	+33.715442	-111.849385	743	5	T. George	
V-07 Wildwood	05:05:56	05:16:01	64	+34.033953	-118.451450	19	5	I. Turk, J. A. Wise	Scan lines present throughout
V-08 Gimple	···	···	···	(+40.137500)	(-120.866667)	(1075)	0	B. Gimple	Bad Weather

NOTE—All site locations are referenced to the WGS84 datum. Positions for sites with no data report the nominal team location (shown with enclosed parentheses) and the team leader(s). *The Canadian sites (Anarchist here) observed using a QHY camera rather than the standard RECON video camera, so and the exposure time is expressed in seconds rather than Sense-Up.

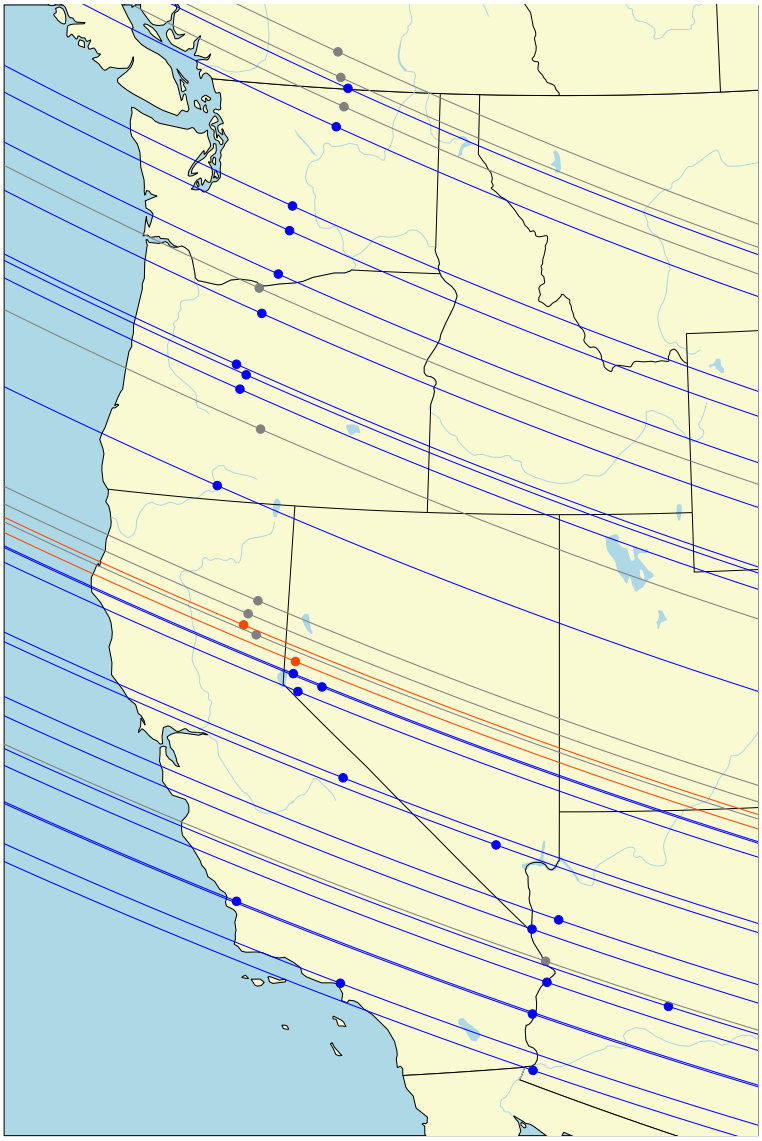

Figure 3. Map of RECON coverage and results across the western United States for the occultation by 2014 YY49 on 2019 January 1. The circular markers indicate the location of each observing team, while the tracks indicate each site's coverage in the down-track direction of the object's shadow. The blue markers indicate good data, with a clear non-detection. The red markers indicate sites which detected an occultation. The gray markers indicate sites which set up but did not record useful data.

3.2. *2013 NL24*

This event was observed as an official campaign for RECON. Twenty-nine teams attempted to observe this occultation. Twenty-four of these teams recorded using the standard RECON recording setup, while 5 of these teams attempted to record using some combination of standard and non-standard equipment (CanCON and other non-official volunteer sites). Of the 29 teams that attempted to observe this occultation, 18 successfully recorded the target star at the predicted time of the occultation to provide constraining data on the target. Of the remaining 11 teams, 2 recorded the

incorrect field, 5 were unable to record due to sky conditions, and 4 were unable to record due to technical issues. Because of the target star was dim, we asked that each team record at a Sense-Up of x128 ($\sim$ 2 second exposures, the longest possible with the RECON MallinCAM cameras). Like the other event described above, each team was asked to record the field over 5x the 1-sigma time uncertainty. A summary of observers is provided in table 5. A map showing RECON's coverage of this event is shown in figure 4.

Table 5. Participating Sites

SiteID	UT start	UT end	SUP	Lat	Lon	Alt	Q	Observers	Comment
1-02 Cedarville	07:03:16	07:16:46	128	+41.528983	-120.177317	1415	5	T. Miller, B. Cain	
1-03 Burney	···	···	···	(+41.045917)	(-121.398990)	(1012)	0	M. Von Schalscha	Technical Issues
1-06 Quincy	07:03:26	07:16:45	128	+39.944577	-120.946692	1021	5	R. Logan, W. Anderson	
1-09 Carson City	07:03:23	07:16:42	128	+39.185675	-119.796470	1510	1		
1-10 Yerington	···	···	···	(+38.991111)	(-119.160833)	(1340)	0	T. Hunt	bad weather
1-12 Tonopah	07:03:55	07:16:35	128	+38.071945	-117.227500	1890	0	J. Martin, R. Gartz, B. Reid	Unable to identify field
2-01 Lee Vining	···	···	···	(+37.961148)	(-119.121267)	(2060)	0	E. Brown	
2-04 Indian Springs	07:03:39	07:16:35	128	+36.440268	-115.357598	878	5	S. Bock	
2-06 Searchlight	07:03:06	07:16:31	128	+35.469015	-114.900348	1061	5	C. Wiesenborn	
2-11 Parker	07:03:05	07:17:13	128	+34.141085	-114.288340	109	0	R. Reaves	
2-12 Idyllwild	07:03:18	07:16:38	128	+33.734320	-116.713512	1688	3	A. Singleton, C. Nelson, E. Smith, Z. French, J. Gombar	
2-13 Blythe	07:03:11	07:16:30	128	+33.607953	-114.577890	55	0	D. Barrows, N. Patel, W. Lechausse	
2-14 Calipatria	···	···	···	(+33.125116)	(-115.524480)	(-56)	0	K. McCandless, C. Settlemire, C. Lara, J. Ballisteros, J. Sanchez, E. Daffern, J. Bustos, J. Cota	Recording failed
2-15 Yuma	07:03:20	07:16:36	128	+32.668015	-114.406025	73	5	D. Thompson, K. Conway, D. Conway	
2-19 Ellensburg	07:03:23	07:16:00	128	+47.002215	-120.540090	487	4	M. Mattes, J. McRae, M Rivard, D. Marshall, B. Palmquist	

Table 5 *continued on next page*

Table 5 *(continued)*

SiteID	UT start	UT end	SUP	Lat	Lon	Alt	Q	Observers	Comment
2-20 Toppenish	···	···	···	(+46.373768)	(-120.394609)	(240)	0	G. Van Doren	Recorded wrong field
2-21 The Dalles	07:03:44	07:17:00	128	+45.588625	-121.160838	121	5	B. Dean, M. Dean	
2-24 Bend	07:03:00	07:17:40	128	+44.132633	-121.331615	971	5		
2-29 Klamath Falls	···	···	···	(+42.224867)	(-121.781670)	(1252.0)	0	S. Anthony, Y. Yang	Technical Issues
3-02 Okanogan	07:02:20	07:18:10	128	+48.362473	-119.596963	296	5	D. Colbert, J. Cheeseman	
3-03 Chelan	07:03:09	07:16:46	128	+47.834232	-120.000437	341	5	R. Jones, N. Lund	
3-05 Yakima	07:02:25	07:18:35	98	+46.602967	-120.544467	351	4		
3-07 Maupin	07:03:18	07:16:38	128	+45.177523	-121.079528	303	5	J. Sowell, J. Popchock	
C-03 Penticton	···	···	···	(+49.533727)	(-119.557377)	(355)	0	B. Gowe	bad weather
C-05 Summerland	···	···	···	(+49.599999)	(-119.670005)	(485)	0	D. Gamble	
C-06 Anarchist	···	···	···	(+49.008827)	(-119.362968)	(1087)	0	P. Ceravolo, D. Ceravolo	
V-04 Oregon Obs	07:03:05	07:17:04	64	+43.885312	-121.447908	1249	5	B. Thomas	
V-05 Scottsdale	···	···	···	(+33.715593)	(-111.849345)	(723)	0	T. George	bad weather
V-07 Wildwood	07:00:03	07:17:13	128	+34.033532	-118.453505	20	4	I. Norfolk, R. Baker, J. A. Wise	High light polution.

NOTE—All site locations are referenced to the WGS84 datum. Positions for sites with no data report the nominal team location (shown with enclosed parentheses) and the team leader(s).

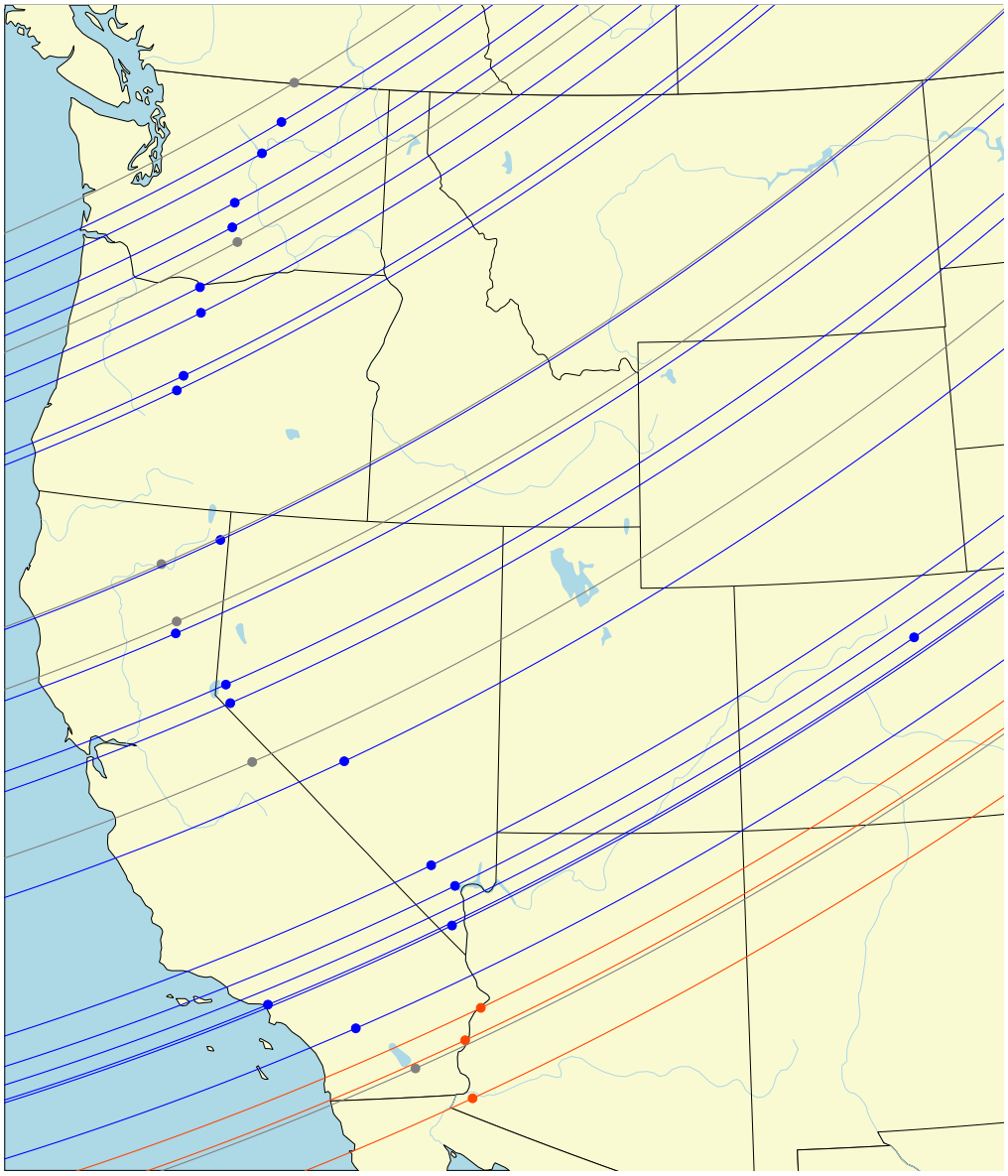

Figure 4. Map of RECON coverage and results for the occultation by 2013 NL24 on 2019 September 4. The circular markers indicate the location of each observing team, while the tracks indicate each site's coverage of the shadow track. The blue sites indicate good data, with a clear non-detection. The red markers indicate sites which detected an occultation. The gray markers indicate sites which set up but did not record useful data.

4. PHOTOMETRIC ANALYSIS

4.1. *MallinCAM CCD Video Data*

Each frame of RECON video data is superimposed by the output of an IOTA-VTI GPS device. This device can be set to display the GPS location of the observing site ("position" mode), or to timestamp each frame with the UT time ("time" mode). A brief video is first recorded in "position" mode, to be used for later analysis steps. The remaining videos, most importantly the event video, are recorded in "time" mode.

The first step in reduction of the data is to extract this timing data. The video files are then converted into FITS frames using a robust average of the frames for a given integration. This step is necessary because the de-interlaced output of the MallinCAM is a .avi video at 29.97 frames per second, regardless of the Sense-Up used, resulting in duplicate frames for any Sense-Up greater than x2. The timing data is corrected as described in Buie & Keller (2016) to reflect the UT midtime of the integration. This is the time used for the final lightcurve analysis. At the same time, the images are dark-subtracted and flat-fielded using calibration videos captured immediately following the event recording. Following these data reduction steps, the FITS frames are ready for lightcurve analysis.

4.2. *QHY CMOS Data*

As a part of the Canadian extension to the RECON network, the Anarchist Mt. Observatory team recorded data for the January event with a QHY174M-GPS. This is the same camera used to obtain the occultation measurement on Arrokoth (Buie et al. 2020). As opposed to the video data recorded by the standard RECON setup, the QHY system writes each single integration directly to a FITS frame, with GPS location and timing data written into the image header. There is no need for dark subtraction as the camera is actively cooled, and at 0° Celsius there is no appreciable dark current over the relatively short exposures used for an occultation campaign. Being a CMOS chip, there is some row-by-row banding visible in the raw data. This is corrected by calculating and subtracting a robust mean from each row in the image - the camera bias and sky signal are also subtracted as a consequence of this. At this point, lightcurve processing can proceed much the same as with the RECON MallinCAM data.

4.3. *Lightcurve Extraction*

Lightcurves are extracted from the FITS data using relative aperture photometry. A suitable anchor star is first chosen to track the motion of the field throughout the video. All other star positions in this field will eventually be tracked via this anchor star. For the first lightcurve extraction, the target star and a number of other reference stars are chosen, and their centroids are automatically tracked to determine the net rotation rate of the field. The lightcurves are then rerun a second time, this time with target and reference positions tracked based on an absolute offset from the anchor star, and a fixed rotation rate about that anchor star. A final relative lightcurve is generated from the target and selected reference stars, with the median relative flux normalized to 1.

4.4. *2014 YY49*

Upon inspection of the resulting lightcurves for this event, it is clear that the lightcurve from (1-08)Reno shows a drop at 05:10:41UT, roughly -0.6σ from the nominal time for that site. This is corroborated by a temporally correlated partial

drop seen in the lightcurve from (1-06)Quincy, less than 20km away in the cross-track direction. Due to cloudy sky conditions, Quincy recorded at a Sense-Up of x128, twice what was requested in the observation materials. As a result of this longer exposure, along with the small size of the object, the star was only occulted for a fraction of an integration, so the drop in the final lightcurve does not drop to zero. The lightcurve from (1-09)Carson City directly to the south showed a clear non-detection, providing a constraint to the southern limb of the object. The closest lightcurve to the north of Quincy was from (1-04)Susanville. This site also showed a non-detection, but because the cross-track distance between Quincy and Susanville is large and the Susanville lightcurve is incredibly noisy, it does not provide a good constraint to the +x cross-track direction. A figure showing all lightcurves from this event is provided (figure 5).

4.5. *2013 NL24*

The lightcurves generated from the data captured for this event indicate a clear positive detection. The three southernmost sites, Parker, Blythe, and Yuma, each recorded a drop in the stellar flux just before the predicted event mid-time. As shown in Figure 14, these drops are well correlated with each other, and take place within 0.2-σ of the nominal mid-time. The lightcurve from Idyllwild shows an evident non-detection, providing a constraint to the northern extent of the object. As the southernmost chord is provided by Yuma, our southernmost RECON site, there is no constraining negative on the southern limb of the object. A figure showing all lightcurves from this event is provided (figure 6).

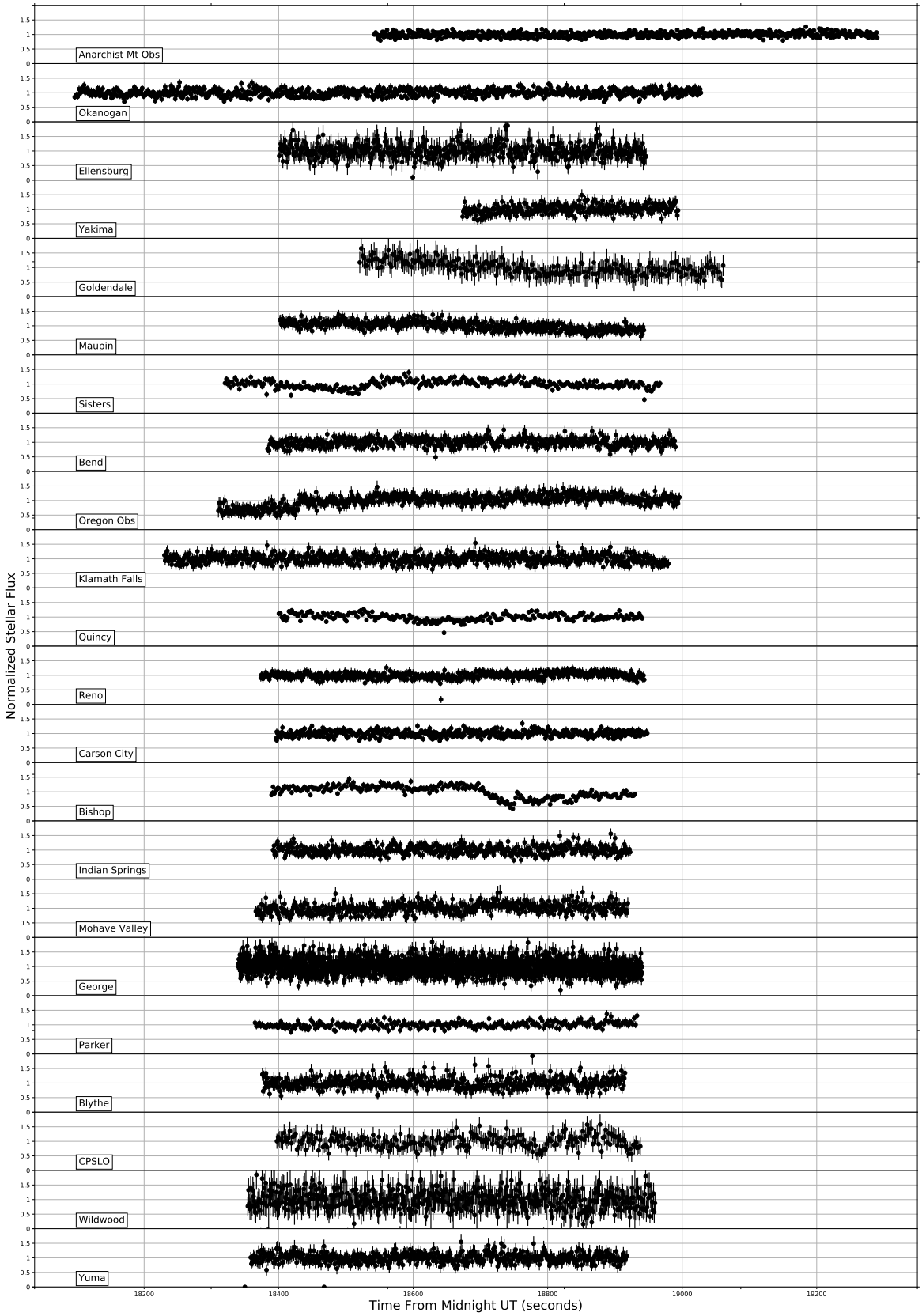

Figure 5. Master figure showing the lightcurve data from RECON sites for the occultation by 2014 YY49. The Occultation is visible in the lightcurves from Reno and Quincy.

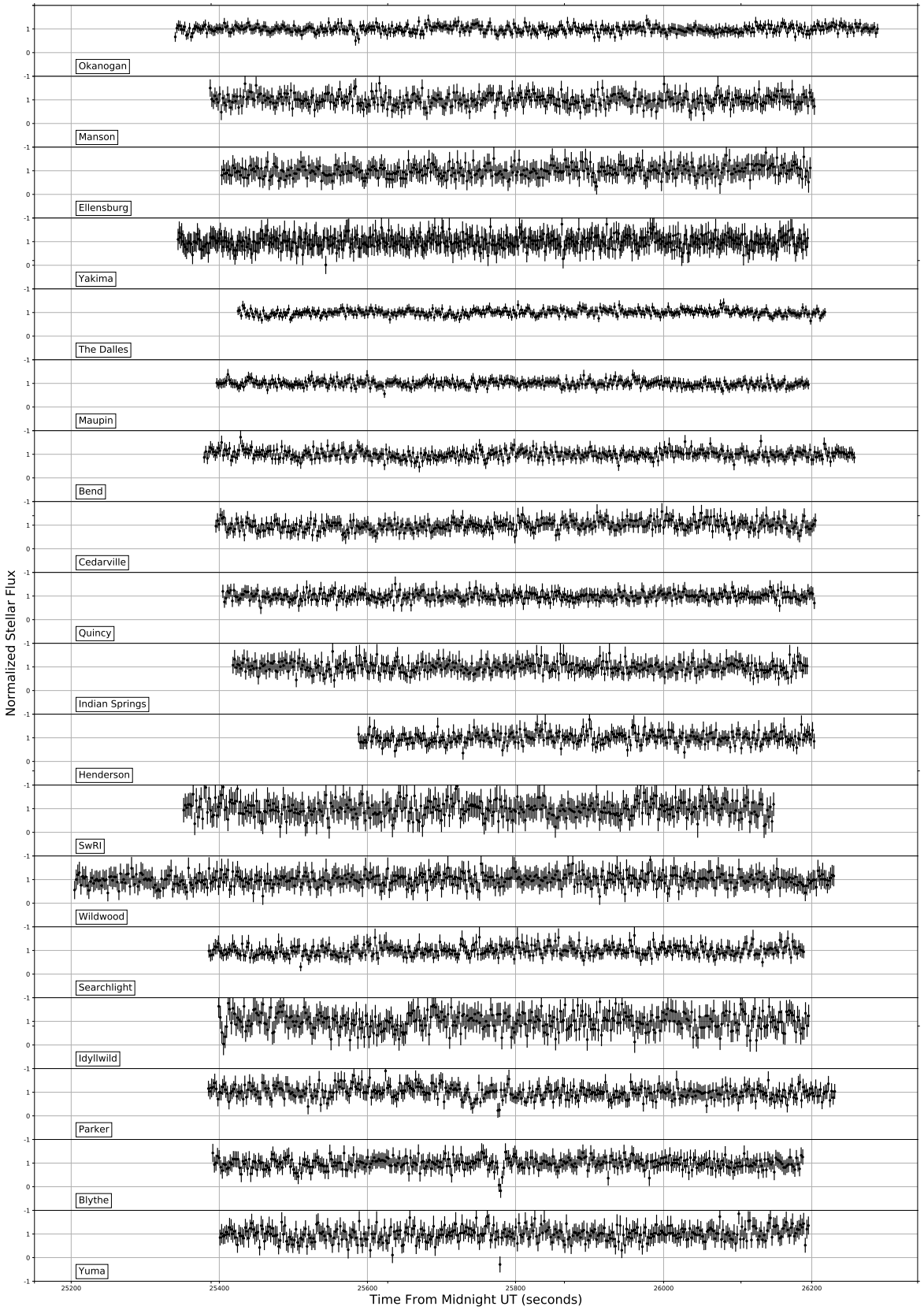

Figure 6. Master figure showing the lightcurve data from RECON sites for the occultation by 2013 NL24. The occultation is visible in the data from (2-11)Parker, (2-13)Blythe, and (2-15)Yuma.

4.6. *Special Case - Gardnerville*

The video from (V-01)Gardnerville for both events suffered from two major issues, neither of which on their own would have significantly impacted the lightcurve extraction process, but both issues together compounded each other such that the standard data processing pipeline described above could not be used for this data set.

The first of these problems was a hardware issue. Over the course of the video recording, a small fraction of frames were dropped and failed to write to the video file. This site observes using a non-standard camera and telescope setup, which may be encoding the video in a non-standard way to cause these dropped frames.

The second of these problems was a failure of the time extraction software. The time extraction procedure reads directly the pixel values at the bottom of the image to determine the UT time that has been stamped onto the frame. This depends on the sky background being appreciably darker than the white text of the time stamp, so that pixels can be easily differentiated. If a bright star is on or near the timestamp, or the sky is too bright, the procedure can fail to do this, and the time extraction will not be successful. In the case of the Gardnerville videos, the time extraction did fail due to stars in the time stamp region of the video.

Ordinarily, for a partially failed time extraction, we would use the successfully time-extracted frames as anchors and interpolate between those to fill in the UT times for those frames on which the extraction failed. Because the camera outputs 29.97 frames per second, each frame's timestamp is expected to be exactly 0.0333667 seconds after the previous frame. This is not true with the videos from Gardnerville, because an undetermined set of frames are missing from this video. Several of these intervals will be greater than this expected interval, and because the time extraction failed on so many frames, it is not feasible to determine where the dropped frames were. Additionally, the averaging of duplicate frames described in subsection 4.1 could not be achieved because there was no way to know which integrations had dropped frames, so a Sense-Up of x2 was used for the extraction. A dummy timefile was generated using the time of the first frame of the video and extrapolating over the number of actual frames, and this timefile was used to extract a raw lightcurve, for the purpose of confirming a non-detection. Because frames were dropped throughout the video, and each integration corresponded to several frames, the probability that all adjacent frames corresponding to a single integration dropped is negligible, so we can with confidence treat these lightcurves as non-detections. Had there been an occultation seen in either of these videos, the timing of each frame around that occultation time would have been extracted by hand so that the rigorous analysis could proceed. The raw lightcurves extracted from these datasets are shown in figures 7 and 8.

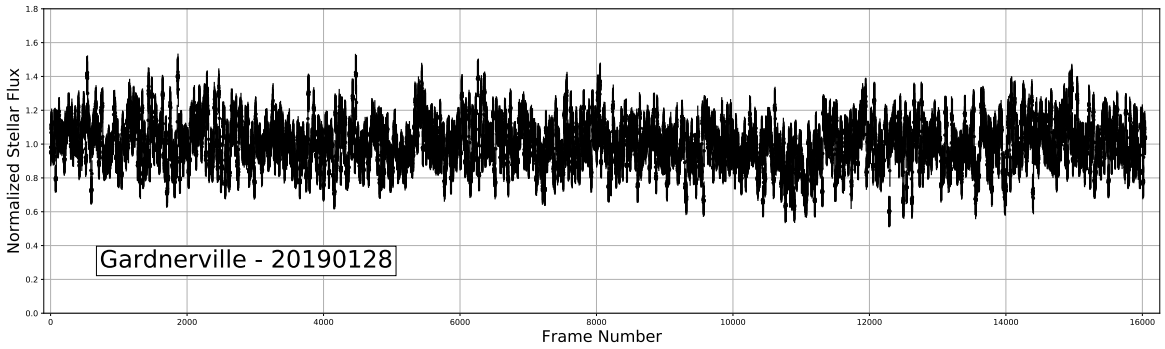

Figure 7. Normalized relative lightcurve generated from the .avi video file provided by Gardnerville for the event involving 2014 YY49. Each data point in this plot is indexed by the frame number, rather than the UT time, because no time extraction was possible. It is clear in this lightcurve that there was no occultation recorded by this site.

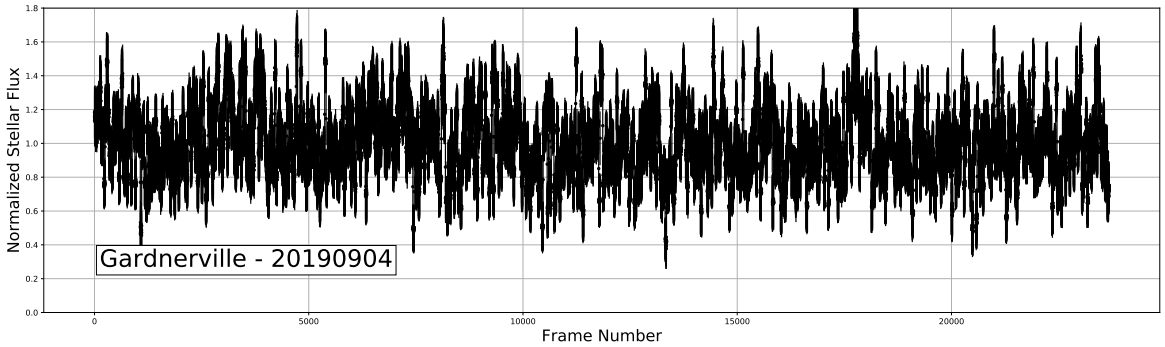

Figure 8. Normalized relative lightcurve generated from the .avi video file provided by Gardnerville for the event involving 2013 NL24. Each data point in this plot is indexed by the frame number, rather than the UT time, because no time extraction was possible. The dip below the noise near frame 13000 corresponds to a small field movement, and there is no corresponding dip from nearby sites, so this is considered a negative. This lightcurve provides a non-detection for this site.

5. PROFILE FITTING

5.1. *2014 YY49*

A statistical Markov Chain Monte Carlo (MCMC) modeling scheme was used to determine a 2-D profile for the object based on lightcurve data. Because there were only two sites with positive detections, and for each of these the star was only occulted for one integration, the data are not sufficiently constraining to allow for any elliptical solution. Therefore, for the profile analysis of the object, sphericity was assumed. For each run of the MCMC, 512 random walkers were used to explore a parameter space in 3 dimensions: the radius of the object, and the 2-dimensional offset of the object's center from the ephemerides. This offset is measured in δx delta δy in the sky-plane as defined in Smart (1977). The osculating orbital parameters used in the MCMC analysis are summarized in table 6. The size distribution for the object radius was truncated between 10km and 60km. The lower limit here is based on the geometrical limits of the two positive detections - In the sky plane, the Reno and

Table 6. Osculating Orbital Elements for 2014 YY49

parameter	value
Epoch*	2019-01-29T00:00:00.000
M	22.73270°±8.9e-05°
ω	193.977636°±7.6e-05°
Ω	188.046823°±2.4e-05°
i	20.406155°±6.2e-06°
e	0.6038219±2.5e-06
a	31.034013±0.000219AU

NOTE—Osculating orbital elements for 2014 YY49 used in the analysis. M, ω, Ω, i, a, e are the mean anomaly, argument of perihelion, ascending node, inclination, eccentricity and semi-major axis respectively.

Quincy chords are not closer than 20km to each other. For a spherical object of this magnitude, a lower geometric albedo limit of 0.01 constrains the radius to less than 60km. Because the size of the object is small (40km) with respect to the 1-σ cross-track uncertainty (738km), and the occultation duration is small compared to the 1-σ timing uncertainty, the positional probability distribution is treated here as uniform. The upper and lower limits of the δx and δy parameters were chosen based on the positions of the constraining negative tracks, and the extents of the chords measured by the positive tracks.

The circular solution was explored with three different prior size distributions. The MCMC was first run with a uniform initial distribution. It was then run assuming size distributions based on a power law with a slope q=3.5, a good match to the size distribution implied by a number of outer solar system surveys (Fraser et al. (2014), Schlichting et al. (2013)). Finally, to cover a broad range of possible power-law distributions, the MCMC was run with a very steep power-law prior size distribution with q=7. For the results reported in this paper, the slope of q=3.5 was used.

The output of the MCMC software is a set of samples distributed within the x-y-r parameter space. A histogram of each parameter provides a probability density function (pdf) for that parameter, and from this pdf, nominal and $\pm 1 - \sigma$ values can be extracted. The MCMC results for 2014 YY49 are shown in figure 9, and summarized in table 8. Figure 10 shows the nominal solutions of the MCMC in the plane of the sky, plotted on top of the lightcurves from the sites used in the analysis. A set of model lightcurves was then generated, with the same site geometry, and assuming the nominal circular profile from the MCMC. Figure 11 shows the resulting model lightcurves plotted along with the actual extracted lightcurves.

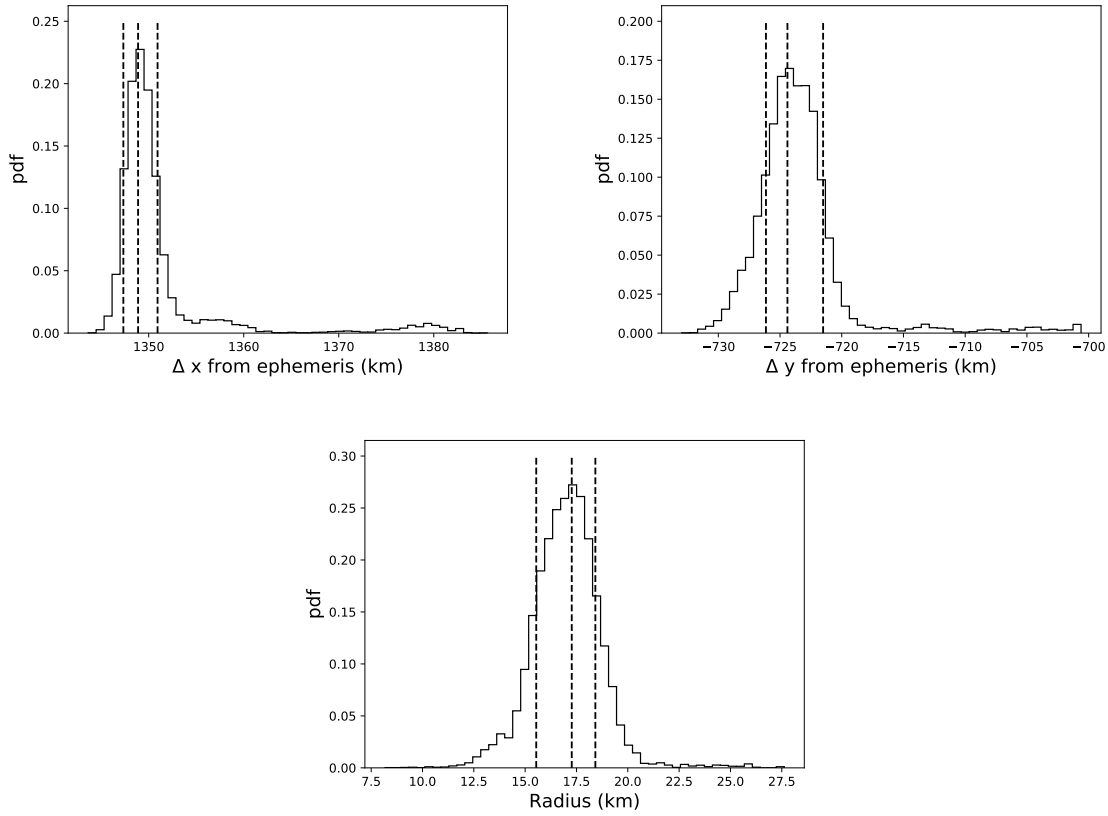

Figure 9. The results of the MCMC for 2014 YY49, with a circular profile assumed. Shown here are probability distribution functions for each of the three free parameters (x offset, y offset, and radius). The vertical dashed lines indicate the nominal value, and the 68% highest density intervals.

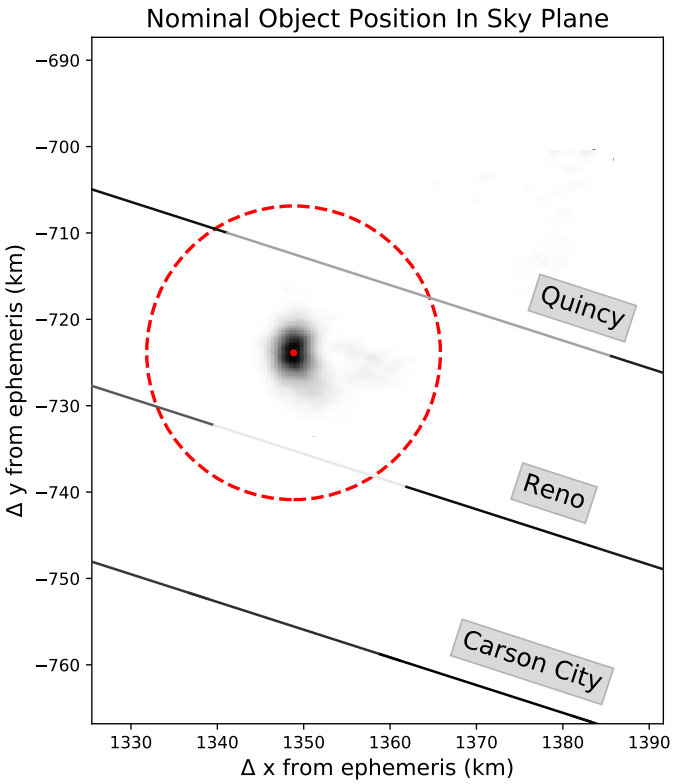

Figure 10. A plot of the circluar object profile for 201 YY49 in the sky plane, based on the results from the MCMC run. The sky plane is defined in a frame of reference moving along with the ephemeris, with the ephemeris as the origin. The black lines show the track of the star in the sky plane for each site. The transparency of each segment corresponds to the relative reduction in stellar flux over that integration. The red circle shows the nominal position and radius of the object, and the dark scatter is the 2-dimensional probability density function for the object's center.

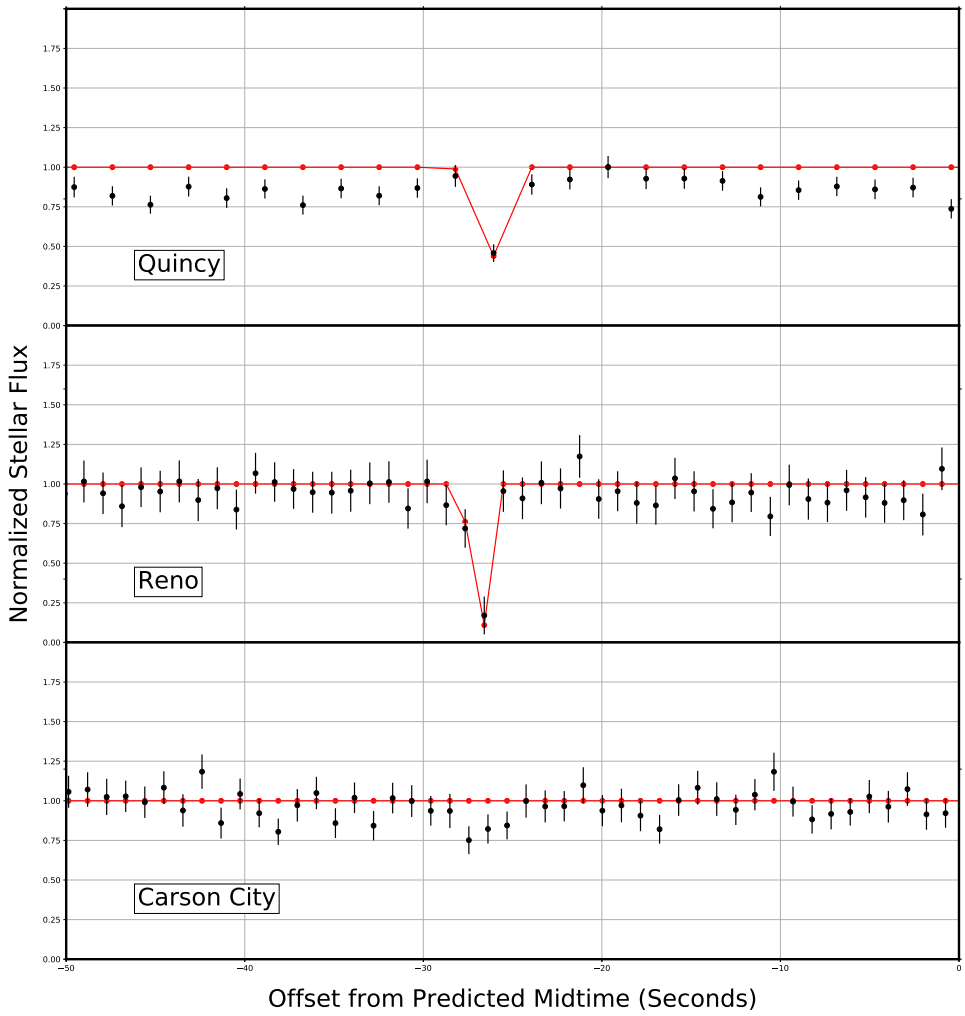

Figure 11. The detection subset of lightcurves from the occultation by 2013 NL24. In black are the lightcurve data points extracted from the RECON video data. Superimposed in red are the hypothetical model lightcurves based on the nominal MCMC results.To correct for the down-track offset between the RECON sites, the time axis is plotted with respect to the predicted event midtime for each site.

5.2. *2013 NL24*

The occultation lightcurve data for this object are much more constraining than those of the other Centaur reported on in this paper, for two reasons: the larger number of chords and the lengths of those chords. Three chords inherently provide more insight into the shape and size of the object than two, as there are far fewer profiles which can be fitted to three chords than two chords. More subtly, the greater length of these chords means that for a given site, the star might have been occulted for more than a single integration. This decreases the fractional uncertainty on the chord lengths by increasing the chord length without increasing the uncertainty on the endpoints of those chords. Additionally, it actually eliminates a source of uncertainty present in the case of a single-integration occultation: with a single-integration occultation, there is no way to know exactly when during that integration the occultation occurred. If, as in the case of the Parker and Blythe data, the star is occulted for more than a single integration, it is immediately known whether a partially occulted integration is the result of an occultation at the beginning or at the end of the integration. The uncertainties in the endpoints of this chord are now only due to the uncertainties in the stellar flux received during the ingress and egress integrations. For this reason, the pdfs from the MCMC were much more symmetric and gaussian than 2014 YY49, and so were the errors. The osculating orbital elements used in the MCMC analysis are summarized in table 7. The results of the MCMC run are shown in figure 12, and summarized in table 8. As with the other object, the geometry of the nominal solution is plotted on top of the lightcurves in figure 13. The nominal circular solution was fed into a program which generates model lightcurves based on the input geometry. Figure 14 shows the resulting model lightcurves plotted on top of the real lightcurves from the video data.

Table 7. Osculating Orbital Elements for 2013 NL24

parameter	value
Epoch*	2019-09-04T00:00:00.000
M	19.034674°±0.000772°
ω	290.076979°±0.001118°
Ω	1.9930136°±0.000275°
i	4.676646°±93.6 mas
e	0.384091±1.3e-05
a	39.976067±0.000994 AU

Note—Osculating orbital elements for 2013 NL24 used in the analysis. M, ω, Ω, i, a, e are the mean anomaly, argument of perihelion, ascending node, inclination, eccentricity and semi-major axis respectively.

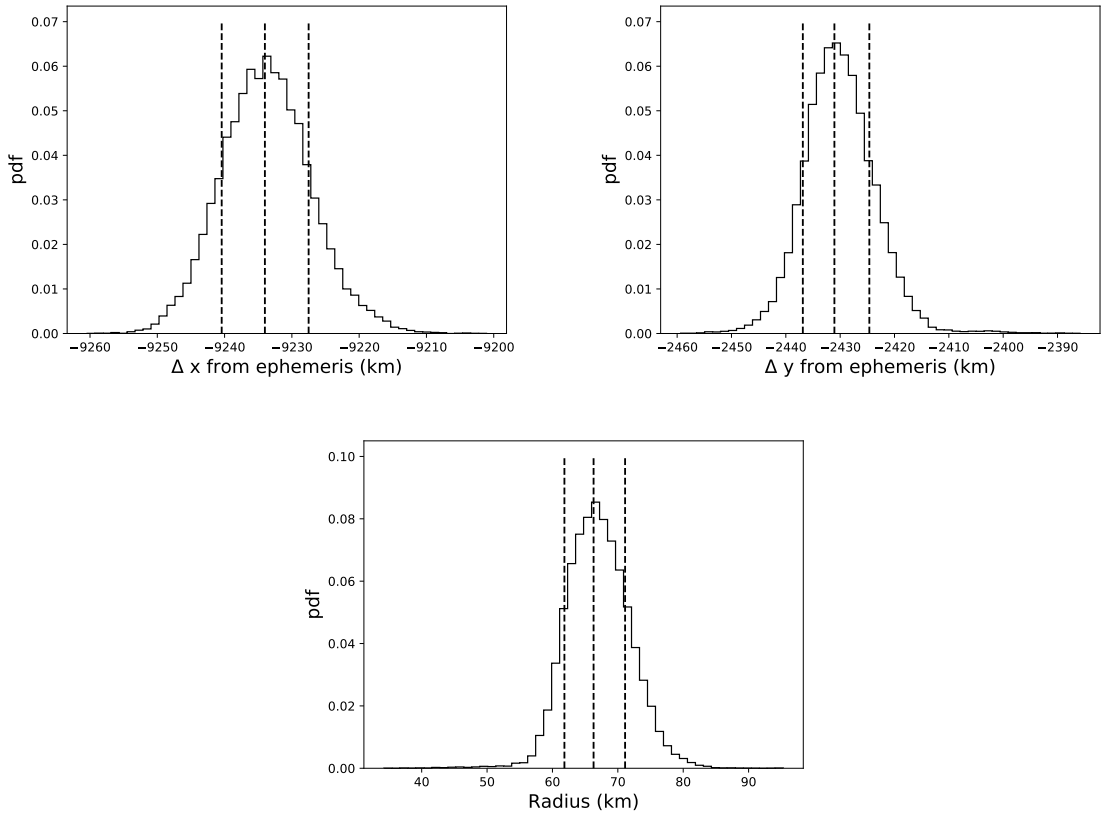

Figure 12. The results of the MCMC for 2013 NL 24, with a circular profile assumed. Shown here are probability distribution functions for each of the three free parameters (x offset, y offset, and radius). The vertical dashed lines indicate the nominal value, and the 68% highest density intervals.

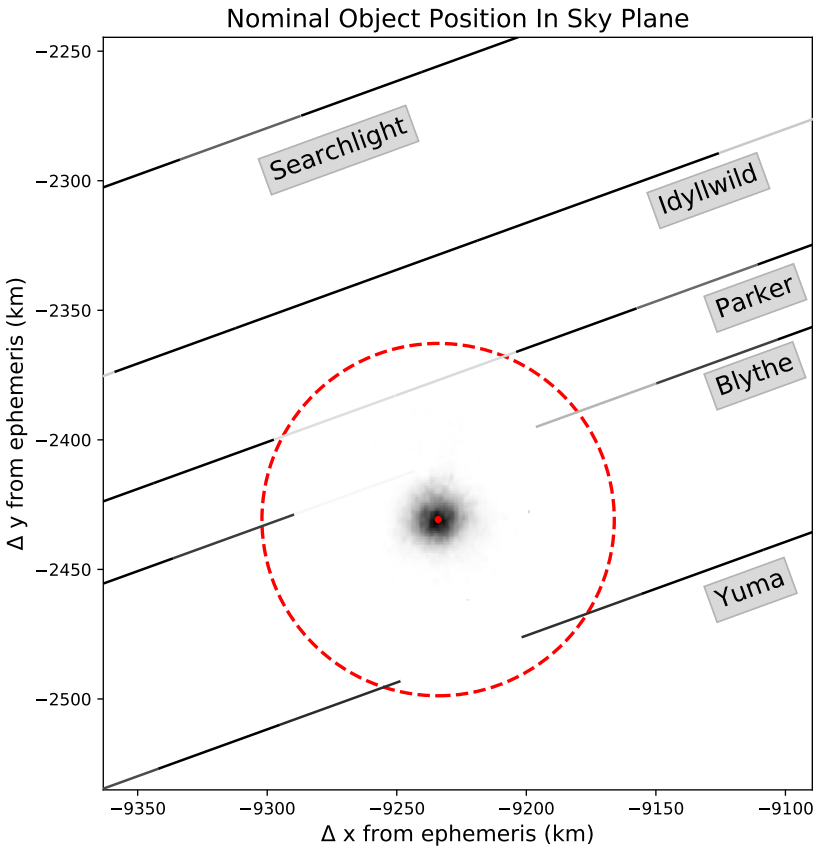

Figure 13. A plot of the circular object profile for 2013 NL24 in the sky plane, based on the results from the MCMC run. The sky plane is defined in a frame of reference moving along with the ephemeris, with the ephemeris as the origin. The black lines show the track of the star in the sky plane for each site. The transparency of each segment corresponds to the relative reduction in stellar flux over that integration. The red circle shows the nominal position and radius of the object, and the dark scatter is the 2-dimensional probability density function for the object's center.

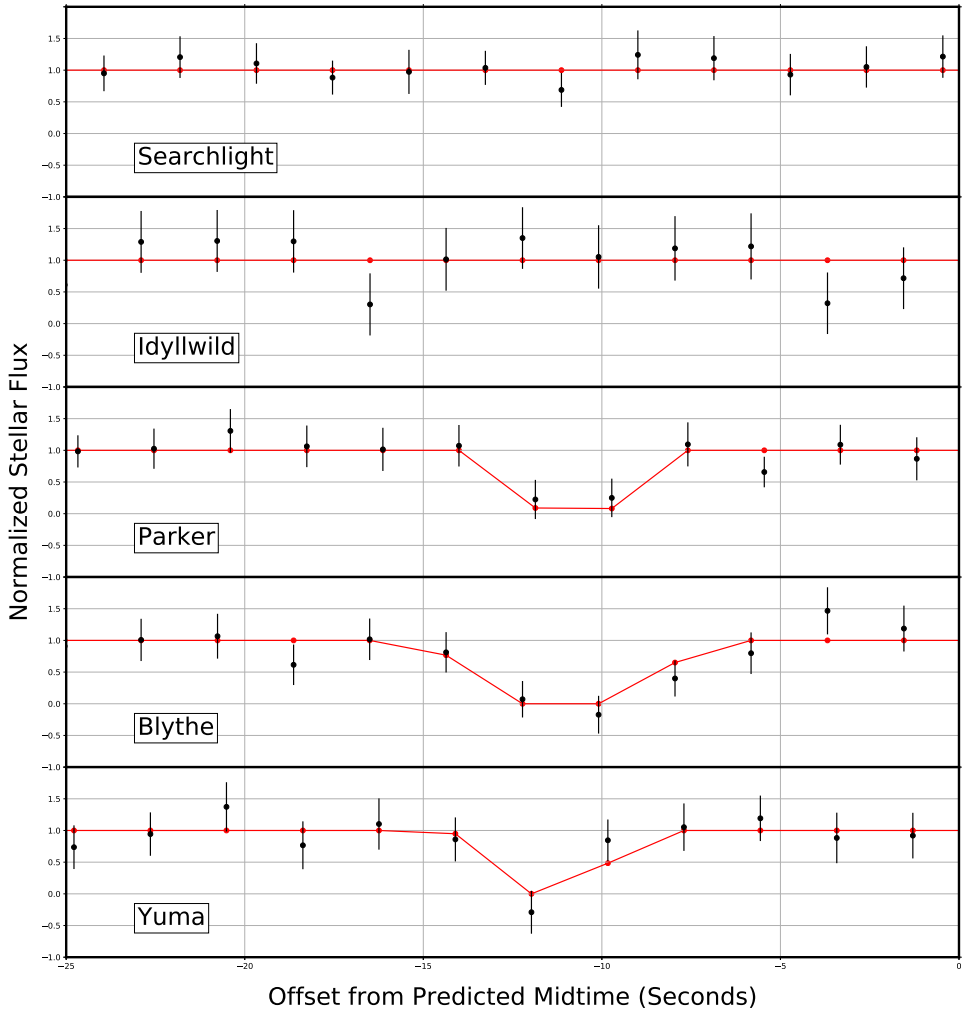

Figure 14. The detection subset of lightcurves from the occultation by 2013 NL24. In black are the lightcurve data points extracted from the RECON video data. Superimposed in red are the hypothetical model lightcurves based on the nominal MCMC results. To correct for the down-track offset between the RECON sites, the time axis is plotted with respect to the predicted event midtime for each site.

Table 8. Results for both objects from the MCMC run

parameter	2014 YY49	2013 NL124
r	$17.21^{+1.21}_{-1.67}km$	$66.29^{+4.82}_{-4.46}km$
Δx	$1348.88^{+2.05}_{-1.55}km$	$-9234.01^{+6.5}_{-6.42}km$
Δy	$-724.4^{+2.89}_{-1.74}km$	$-2431.06^{+6.43}_{-5.81km}$
$\Delta\alpha$	$104.37^{+0.16}_{-0.12}mas$	$-486.00^{+0.34}_{-0.34}mas$
$\Delta\delta$	$-56.07^{+0.22}_{-0.13}mas$	$-130.51^{+0.35}_{-0.31}mas$

NOTE—These offsets are reported with respect to the object ephemerides as of the epochs described in tables 6 and XXX 7. The nominal values reported here are from the peakes of the pdfs from the MCMC. The uncertainties are based on the 68% credible highest density intervals caclulated about these peaks.

6. DISCUSSION

The most informative result obtained here is the radius of each object. A radius measurement by occultation is much more precise than the thermal radiometry measurements used to determine many object radii, and can serve to constrain and corroborate these thermal results. This is not immediately possible for the two objects discussed in this paper, as there have been no prior attempts to determine the size of these objects. Follow-up measurements via thermal radiometry can and should be taken and compared with these occultation results.

We have determined the sizes of these two Centaurs to a relatively high precision with these occultation results. However, the size of the object, (particularly with so few chords as these) is not itself particularly informative of the object's makeup - for this, additional derived parameters are needed, such as geometric albedo, color, and bulk density. Bulk density is the most challenging of these to determine for distant objects, as it requires a measurement of the mass of the object. Aside from a spacecraft encounter, the only way to acquire such a measurement is by observation of a secondary object orbiting the primary. Neither of the two occultation results reported here indicated the presence of a secondary, so mass-determination is not possible.

Albedo on the other hand, can be determined much more easily via additional photometry. Albedo is a derived quantity which can be determined (for a circular object) from just the radius and the absolute magnitude. From the occultation results we have well-constrained measurements of the radii for both Centaurs. The absolute magnitudes H_v are much more poorly constrained - the best values in literature are those provided by the Minor Planet Center (MPC), but these values are rough estimates with no published formal uncertainties (ref XXX). Careful, targeted pho-

tometry to determine these values to high precision is desired as follow-on work to this paper such that, in tandem with the results from the occultations, well-constrained geometric albedos can be obtained.

There is the additional consideration of object rotation in the determination of the albedo. If an elliptical object is rotating in such a way that it's cross- section in the plane of the sky is variable over time, then its measured absolute magnitude will also vary with time. If this is the case, then subsequent photometric measurements may permit the detection of a periodic change in brightness, which could be extrapolated back to the event time to determine the phase of rotation at the time of the occultation, and provide insight into the three-dimensional profile of the object.

There is some interest regarding the colors of these targets as well. A number of papers have reported a clear bimodal color/albedo distribution in the population of KBOs and Centaurs, with the population split between dark grey objects and bright red objects. While no rigorous albedo results are reported in this paper, we can adopt the reported H_v values from MPC and the nominal values for radius to determine an estimate for the geometric albedo of both of these targets. Adopting these values, and defining geometric albedo as $P_v = (\frac{1329*10^{\frac{-H_v}{5}}}{2*r})^2$, we get geometric albedos of $P_v = 0.12$ for 2014 YY49 and $P_v = 0.045$ for 2013 NL24. These values reflect the bimodal albedo distribution reported by Tegler et al. (2016), and follow-on color photometry work will, in the context of these occultation results, provide evidence either supporting or weakening this hypothesis.

Of the most interest to the RECON project is follow-on occultation work. Even with only two or three chords, the astrometric measurement provided by a positive detection by occultation has a precision far beyond any direct astrometric measurement via large telescopes. The astrometry from these occultations will considerably reduce the uncertainty on the orbits of these two objects, and allow for much higher-precision occultation predictions in the future. While RECON is nominally a large, stationary network aimed at low resolution measurements of high-uncertainty events, it is of interest to RECON to explore the feasibility of more targeted, mobile deployments to chase low-uncertainty follow-up occultations based on predictions informed by the astrometric measurements obtained here. As a proof-of-concept for such a campaign, a subset of RECON teams in Oregon, California, and Nevada deployed in October 2019 to successfully observe an occultation by the Jupiter trojan asteroid Leucus, one of the five targets for the upcoming *Lucy* mission. The results of this campaign are currently being analyzed for future publication, but are beyond the scope of this paper.

ACKNOWLEDGMENTS

All data reported on in this work was obtained by the citizen observers who make up the RECON network. the RECON project extends well beyond the observers named in this paper, and without every one of them, the project would not be possible. Funding for RECON was provided by a grant from NSF AST-1413287, AST-1413072, AST-1848621, and AST-1212159. Prediction efforts for RECON are supported by astrometric measurements taken with, among other observatories, the 3.5 meter telescope at the Apache Point Observatory (APO). Many thanks to APO, and the APO observing specialists for assisting with these observations.

REFERENCES

Braga-Ribas, F., Crispim, A., Vieira-Martins, R., et al. 2019, Journal of Physics: Conference Series, 1365, 012024, doi: 10.1088/1742-6596/1365/1/012024

Buie, M. W., & Keller, J. M. 2016, The Astronomical Journal, 151, 73, doi: 10.3847/0004-6256/151/3/73

Buie, M. W., Porter, S. B., Tamblyn, P., et al. 2020

Chambers, K. C., Magnier, E. A., Metcalfe, N., et al. 2016, arXiv e-prints, arXiv:1612.05560. https://arxiv.org/abs/1612.05560

Fraser, W. C., Brown, M. E., Morbidelli, A., Parker, A., & Batygin, K. 2014, The Astrophysical Journal, 782, 100, doi: 10.1088/0004-637x/782/2/100

Horner, J., Evans, N. W., & Bailey, M. E. 2004, MNRAS, 354, 798, doi: 10.1111/j.1365-2966.2004.08240.x

Lebofsky, L. A., & Spencer, J. R. 1989, in Asteroids II, ed. R. P. Binzel, T. Gehrels, & M. S. Matthews, 128–147

Lindegren, L., Hernández, J., Bombrun, A., et al. 2018, Astronomy & Astrophysics, 616, A2, doi: 10.1051/0004-6361/201832727

Schlichting, H. E., Fuentes, C. I., & Trilling, D. E. 2013, The Astronomical Journal, 146, 36, doi: 10.1088/0004-6256/146/2/36

Smart, W. M. 1977, Textbook on Spherical Astronomy, 6th edn. (Cambridge University Press)

Spencer, J. R., Stern, S. A., Moore, J. M., et al. 2020, Science, 367, aay3999, doi: 10.1126/science.aay3999

Tegler, S. C., Romanishin, W., Consolmagno, G. J., & J., S. 2016, AJ, 152, 210, doi: 10.3847/0004-6256/152/6/210

Timerson, B., Durech, J., Aguirre, S., et al. 2009, Minor Planet Bulletin, 36, 98